

# The Influence of Large-Scale Spatial Warming on Jet Stream Extreme Waviness on an Aquaplanet

T. J. Batelaan<sup>1</sup>, C. Weijenborg<sup>1</sup>, G.J. Steeneveld<sup>1</sup>, C. C. van Heerwaarden<sup>1</sup>,  
V. A. Sinclair<sup>2</sup>

<sup>1</sup>Meteorology and Air Quality Section, Environmental Sciences Group, Wageningen University, P.O. Box 47, 6700 AA Wageningen, The Netherlands

<sup>2</sup>Institute for Atmospheric and Earth System Research/Physics, Faculty of Science, University of Helsinki, P.O. Box 64, 00014, Helsinki, Finland

## Key Points:

- Weakened jet streams do not become wavier on an aquaplanet with reduced temperature gradients due to warming in mid- and high latitudes
- The magnitude of large wave amplitudes and jet stream extreme waviness decrease robustly under large-scale spatial warming on an aquaplanet

---

Corresponding author: Thomas J. Batelaan, [thomas.batelaan@wur.nl](mailto:thomas.batelaan@wur.nl)

**Abstract**

14 The effect of modified equator-to-pole temperature gradients on the jet stream by low-  
15 level polar warming and upper-level tropical warming on jet streams is not fully under-  
16 stood. We perform four aquaplanet simulations to quantify the impact of different sea  
17 surface temperature distributions on jet stream strength, wave amplitudes and jet stream  
18 waviness, quantified by a modified Sinuosity Index. A large-scale uniform warming sce-  
19 nario increases the jet strength whereas decreases in jet strength occur in two scenar-  
20 ios where the meridional temperature gradient is reduced. However, all scenarios indi-  
21 cate substantial decreases in the magnitude of large wave amplitudes, jet stream extreme  
22 waviness and reduced variability of these diagnostics, suggesting a relationship with weak-  
23 ened baroclinicity. Our findings contradict the earlier proposed mechanism that low-level  
24 polar warming weakens the jet stream and increases wave amplitudes and jet stream wavi-  
25 ness. We conclude that a weaker jet stream does not necessarily become wavier.  
26

**Plain Language Summary**

27 This research letter considers how different patterns of atmospheric warming, like  
28 low-level warming at the poles and at high altitude in the tropics, impact the jet stream,  
29 which is a strong ‘river’ of high-altitude wind. We use numerical model simulations to  
30 mimic different scenarios of warming that maintain or reduce the temperature gradient  
31 between equator and poles. We find that when an Earth-like planet completely covered  
32 by water warms in specific ways, it strengthens or weakens the jet stream, but reduces  
33 the size of its largest waves, and makes the extreme waviness episodes less wavy. We ex-  
34 plain that this is possibly related to the reduced energy available to grow weather sys-  
35 tems. Furthermore, this research letter conclude that weakened jet streams do not nec-  
36 essarily become wavier, which is against the idea that weakened jet streams become wavier  
37 due to warming in polar regions.  
38

## 1 Introduction

Key characteristics of anthropogenic global warming are polar amplification and upper tropospheric tropical warming (e.g., IPCC, 2021; Gulev et al., 2021; Lee et al., 2021; Doblas-Reyes et al., 2021). These large-scale spatial warming phenomena alter the equator-to-pole temperature gradient in the lower and upper troposphere, which, in turn, initiates the “meridional tug-of-war on the jet stream” (Barnes & Screen, 2015; Shaw et al., 2016; Stendel et al., 2021).

The impact of the altered meridional temperature gradients on the jet stream remains a subject of ongoing research (e.g., Coumou et al., 2018; Vavrus, 2018; Cohen et al., 2020). Recently, Woollings et al. (2023) found that the observed weak poleward jet shift could be potentially linked to upper tropospheric tropical warming. However, most studies focus on the influence of amplified Arctic warming on the jet stream and several hypotheses have been put forward (see e.g., Cross-Chapter Box 10.1 Doblas-Reyes et al., 2021). For instance, Francis and Vavrus (2012, 2015) hypothesized that a weaker jet stream, caused by polar amplification, would become more wavy, potentially leading to more frequent weather extremes. This hypothesis is that a wavy jet stream is associated with atmospheric blocking and Rossby wave breaking, which are known to be related to mid-latitude weather extremes (Woollings et al., 2018). While this hypothesis has generated much discussion over the past decade, it has yet to be conclusively confirmed or refuted (e.g., Barnes, 2013; Barnes & Screen, 2015; Cohen et al., 2020).

Most studies about projected waviness changes with comprehensive climate models indicate a decrease in waviness (Barnes & Polvani, 2015; Cattiaux et al., 2016; Peings et al., 2017) but with a large intermodel spread. To disentangle processes in highly nonlinear climate models, numerous studies have attempted to replicate Arctic amplification through prescribed sea-ice loss in climate models and test the influence on circulation (Screen et al., 2018; Smith et al., 2019). However, the findings of these studies are still inconclusive, confirming the link (Mori et al., 2019), noting no clear differences in waviness (e.g., Ogawa et al., 2018; Blackport & Screen, 2020) or showing weak responses to sea-ice loss (Smith et al., 2022). To even further reduce complexity in the search of causality, highly idealized modeling studies have investigated the impact of changes in the meridional temperature gradient alone. However, they have focused on migration of the storm track (Butler et al., 2010), on the effect of blocking (Hassanzadeh et al., 2014) and temperature variability (Schneider et al., 2015) rather than on waviness changes. Schemm and Röthlisberger (2024) do study jet stream waviness changes, however only under uniform warming.

This research letter focuses on changes of jet stream extreme waviness, associated with large amplitude waves and weather extremes, in an highly idealized model framework. We have conducted four simulations with the OpenIFS model in aquaplanet configuration in which we have increased the Sea Surface Temperatures (SSTs) while either maintaining or reducing the meridional gradients. Compared to previous highly idealized studies (Butler et al., 2010; Hassanzadeh et al., 2014) we retained moist processes that can yield significant feedback on the dynamics (Vallis, 2020). Moreover, a more realistic mean temperature distribution and meridional temperature gradient reductions are established compared to previous studies (Hassanzadeh et al., 2014; Schneider et al., 2015).

Conducting these simulations, we aim to determine the influence of large-scale spatial warming on jet stream extreme waviness. We first discuss the modeled influence of the altered SSTs on the zonal mean temperature distribution and the atmospheric jet. Thereafter we discuss if the changed mean state possibly leads to changes in the largest amplitudes of the waves in the jet stream, jet stream extreme waviness and cut-off segments related to blocking highs and cut-off lows that are associated with weather extremes (Cattiaux et al., 2016).

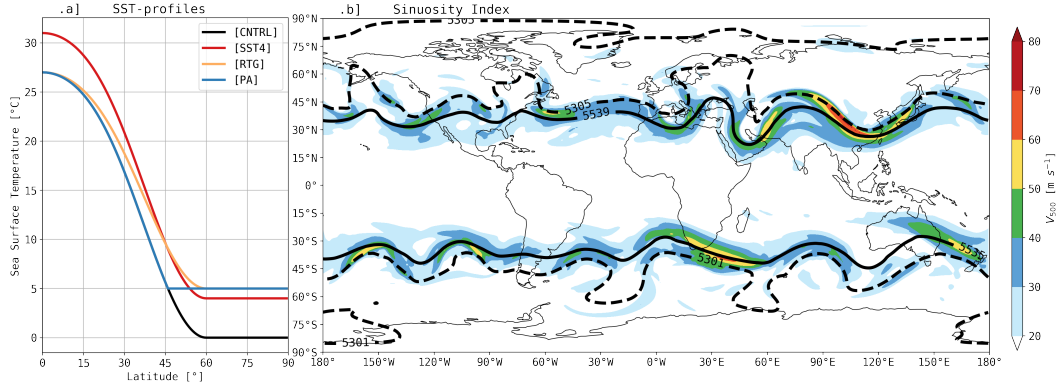


**Figure 1.** a) Prescribed SST [ $^{\circ}\text{C}$ ] profiles as a function of latitude for the four model experiments. The profiles are zonally uniform and symmetric about the equator. b) Sinuosity Index [-] visualized for a selected timestep of the [CNTRL]-simulation. The black dashed contour line is the average  $Z500$  isohypse [m] based on the original  $SI$  metric and the black solid contour line is the average  $Z500$  isohypse based on our modified  $SI$  method. Shading denotes the 500-hPa wind speed [ $\text{m s}^{-1}$ ]. Coastlines are included for reference, but are nonexistent in the simulations.

## 91 2 Methods

### 92 2.1 OpenIFS

93 We use the numerical weather prediction model OpenIFS, developed by the Eu-  
 94 ropean Center for Medium Range Weather Forecasts (ECMWF). OpenIFS shares the  
 95 same dynamical core and physical parametrizations as the Integrated Forecast System  
 96 (IFS) which is used for operational weather forecasting at ECMWF. However, compared  
 97 to IFS, OpenIFS lacks data assimilation capacity and is not coupled to an ocean model.  
 98 We use version Cy43r3v2 that was operational between July 2017 and June 2018 (docu-  
 99 mentation online at <https://www.ecmwf.int/en/publications/ifs-documentation>).

### 100 2.2 Experimental Setup

101 The experimental setup and initial conditions follow Sinclair and Catto (2023). The  
 102 simulations run in the aquaplanet configuration with fixed zonally uniform SSTs. The  
 103 incoming solar radiation is specified at the equinoctial value to remove seasonal varia-  
 104 tion, but a diurnal cycle is present. The simulations run at T255 resolution (grid spac-  
 105 ing of about 78 km at the equator) and with 60 vertical model levels with the model top  
 106 at 0.1 hPa. The initial conditions are modified from a randomly selected real atmospheric  
 107 state from the ERA5-reanalysis (Hersbach et al., 2020). First, the land-sea mask is changed  
 108 to cover the whole globe by ocean. Second, the surface geopotential is set to zero every-  
 109 where. Finally, the atmospheric fields are interpolated to the new flat surface in regions  
 110 where there is topography on Earth.

111 We conduct four experiments, i.e. [CNTRL], [SST4], and [PA] following Sinclair  
 112 and Catto (2023) and an additional Reduced Temperature Gradient [RTG] simulation.  
 113 The simulations are selected because compared to [CNTRL] they establish large-scale  
 114 spatial warming with upper tropical warming in [SST4], polar amplification in [PA] and  
 115 gradual warming from the equator resulting in a large meridional temperature gradient  
 116 reduction in [RTG]. Through executing these four simulations we are able to study the  
 117 impact of large-scale spatial warming on jet stream waviness.

118 The control simulation [CNTRL] follows the SST-profile QObs of Neale and Hoskins  
 119 (2000) that tries to resemble Earth's SSTs. It has maximum SSTs of 27°C on the equa-  
 120 tor decreasing poleward to 0°C at 60° latitude from where they remain constant (Fig-  
 121 ure 1a). The [SST4] simulation has a uniform warming of 4°C compared to the [CNTRL]  
 122 simulation (Figure 1a). This results in upper tropical warming (Sinclair et al., 2020; Sin-  
 123 clair & Catto, 2023). The polar amplification simulation [PA] (AA in Sinclair & Catto,  
 124 2023) uses the QObs SST distribution between 45°S and 45°N, with SSTs set to 5°C pole-  
 125 ward of these latitudes to mimic polar amplification (Figure 1a). Compared to [CNTRL]  
 126 the SSTs of the [RTG] simulation are gradually warmed from the equator with the max-  
 127 imum temperature increase of 5°C occurring poleward of 60° latitude (Figure 1a). This  
 128 additional simulation is conducted to simulate a more realistic equator-to-pole temper-  
 129 ature gradient reduction, with warming occurring in the subtropics, mid-latitudes, and  
 130 polar regions, rather than just at high latitudes as in the [PA] simulation.

131 Each simulation is run for a total of 11 years. This simulation length is long enough  
 132 to capture internal variability as there is no seasonal cycle in our simulations. However,  
 133 to ensure a balanced state is achieved, the first year of each simulation is discarded. Model  
 134 output is saved every six hours on 22 pressure levels between 1000 hPa and 10 hPa.

### 135 2.3 Jet Stream Waviness Quantification

136 To quantify waviness different methods exist (e.g. Francis & Vavrus, 2012; Chen  
 137 et al., 2015; Cattiaux et al., 2016; Di Capua & Coumou, 2016; Röthlisberger, Martius,  
 138 & Wernli, 2016; Martin, 2021). Dynamical approaches use concepts based on energy con-  
 139 servation while geometric approaches aim to capture the shape of the waves (Vavrus, 2018).  
 140 We use the geometric *Sinuosity Index* (*SI*) by Cattiaux et al. (2016) because their method  
 141 includes cut-off segments related to blocking highs and cut-off lows and has been used  
 142 in conjunction with the Local Wave Activity metric (Chen et al., 2015) without diver-  
 143 gent outcomes (Blackport & Screen, 2020). Moreover, the *SI* method is defined at the  
 144 500 hPa pressure level that has the advantage to be insensitive to heating (Barnes, 2013;  
 145 Cattiaux et al., 2016). *SI* is computed every 6 hours to capture synoptic-scale variabil-  
 146 ity.

147 Cattiaux et al. (2016) compute the *SI* as a measure of the mean flow around 50°  
 148 latitude. First they calculate the average 500-hPa geopotential height,  $Z_{500}$ , between  
 149 30° and 70° latitude. Then, Cattiaux et al. (2016) define the *SI* as the ratio between the  
 150 length of the isohypse with the estimated  $Z_{500}$  value to the circumference of the Earth  
 151 at 50° latitude.

152 Unfortunately, the original *SI* metric does not adequately capture the jet stream  
 153 in the aquaplanet setup (Figure 1b). Specifically, the isohypse do not align well with the  
 154 wind maxima associated with the jet stream and also contains segments at high latitudes  
 155 that are unrelated to the jet stream or atmospheric blocks. To address this issue, we de-  
 156 velop a new method to determine the latitudinal range  $\Delta\phi$  over which to calculate the  
 157  $Z_{500}$  average. Specifically, we identify  $\Delta\phi$  in each hemisphere where the time mean zonal  
 158 mean magnitude of the horizontal wind vector at 500 hPa  $[\overline{V}_{500}]$  exceeds half of its cli-  
 159 matological maximum of  $[\overline{V}_{500}]$  (Figure S1), where the overbar represents time mean and  
 160 square brackets denoted the zonal mean. By using this method, we find the following  
 161 latitude ranges per simulation per hemisphere: (21.4°N, 47.4°N) & (22.1°S, 47.4°S) for  
 162 the [CNTRL]-simulation, (22.8°N, 51.6°N) & (22.1°S, 51.6°S) for the [SST4] simulation,  
 163 (20.7°N, 49.5°N) & (21.4°S, 49.5°S) for the [RTG] simulation and (20.7°N, 45.3°N) & (21.3°S,  
 164 45.3°S) for [PA]. We find the same latitude ranges if we use the zonal mean zonal wind  
 165 ( $[\overline{u}_{500}]$ ) instead of  $[\overline{V}_{500}]$ . Between the above mentioned latitudinal ranges we calculate  
 166 the average  $Z_{500}$  at every timestep which is then used as the selected value of the iso-  
 167 hypse to calculate its length.

168 Moreover, Cattiaux et al. (2016) use a constant normalization of circumference of  
 169 the Earth at 50° latitude, but to account for the latitudinal jet stream migration we nor-  
 170 malize the length of the Z500 isohypse with the circumference of the Earth at the mean  
 171 latitude of the selected isohypse  $\tilde{\phi}_{Z500}$ . The resulting modified  $SI$  is defined as follows:

$$172 \quad SI(\phi, t) = \frac{\text{arclength}(Z500_{\Delta\phi}(t))}{2\pi a \cos(\tilde{\phi}_{Z500}(\phi, t))}, \quad (1)$$

173 where  $Z500_{\Delta\phi}$  is the average geopotential height at 500 hPa between the above men-  
 174 tioned latitudinal ranges per simulation per hemisphere  $\Delta\phi$ ,  $a$  denotes the radius of Earth  
 175 and  $\tilde{\phi}_{Z500}$  is the mean latitude of the selected Z500 isohypse. A value of  $SI=1$  indicates  
 176 a straight westerly atmospheric flow, whereas  $SI$  values in the range 2-3 indicate a strongly  
 177 meandering flow with the average Z500 isohypse being 2-3 times longer than the circum-  
 178 ference of the Earth at the mean latitude.

179 Further, we use the meridional extent defined as the difference between the max-  
 180 imum and minimum latitude of the selected Z500 isohypse, to quantify the wave am-  
 181 plitude (Barnes, 2013). Moreover, the  $SI$  metric enables the possibility to differentiate  
 182 between the circumglobal isohypse and cut-off segments related to blocking highs and  
 183 cut-off lows that are associated with weather extremes, as shown by Cattiaux et al. (2016).  
 184 We only maintain cut-off segments that are larger than the circumference of a circle with  
 185 radius of 78 km (i.e. 1 grid cell).

### 186 **3 Mean State Response in Temperature (gradient) and Zonal Wind**

187 All simulations display zonal mean climatologies of temperature and zonal wind  
 188 that are generally consistent with observations of the Earth's atmosphere (Figure 2, row  
 189 1 and 3). The core of the jet streams are located near 30° latitude at tropopause level.  
 190 The dynamical tropopause, defined as the 2 PVU-surface, has physically plausible val-  
 191 ues that vary between 100 hPa in the tropics and 300 hPa at the poles (Figure 2). The  
 192 simulations exhibit almost perfect symmetry, as would be expected from the aquaplanet  
 193 set up.

#### 194 **3.1 [SST4] simulation**

195 The [SST4] simulation reveals the most substantial tropospheric warming of all sim-  
 196 ulations. Climatological temperature increases of over 5 K are ubiquitous (Figure 2a).  
 197 The warming signal is particularly strong in the upper tropical troposphere, exceeding  
 198 10 K due to enhanced latent heat release in the rising branch of the Hadley cells (not  
 199 shown). The tropospheric warming leads to a deeper troposphere, as indicated by the  
 200 lifted dynamic tropopause (Figure 2, column 1). Furthermore, the lower polar strato-  
 201 sphere cools, which is potentially due to a weakened Brewer-Dobson circulation.

202 The combined impact of the deeper troposphere, upper tropospheric tropical warm-  
 203 ing and lower stratospheric polar cooling in the [SST4] simulation results in an enhanced  
 204 meridional temperature gradient around 200 hPa (Figure 2d). The most significant in-  
 205 crease in the meridional temperature gradient occurs at approximately 25° latitude at  
 206 tropopause level. Wind speeds in the core of the subtropical jet stream strengthened con-  
 207 sistently by approximately 6%, from 53.3 m s<sup>-1</sup> to 56.9 m s<sup>-1</sup>. The core of the jet stream  
 208 also shifts upward by 25 hPa, from 175 hPa in [CNTRL] to 150 hPa in the [SST4] sim-  
 209 ulation. However, stronger increases exceeding 10 m s<sup>-1</sup> in zonal wind occur above the  
 210 jet stream cores due to an increase in the jet stream height, consistent with the increase  
 211 height of the tropopause (Figure 2g). The upward shift of the jet core is also evident by  
 212 the decrease in the zonal wind speed below the jet core in the (sub)tropical regions. In  
 213 addition to the deeper zonal wind distribution, we also find a poleward shift in the jet  
 214 stream position caused by an expanding tropical atmosphere. The tropical warming pushes

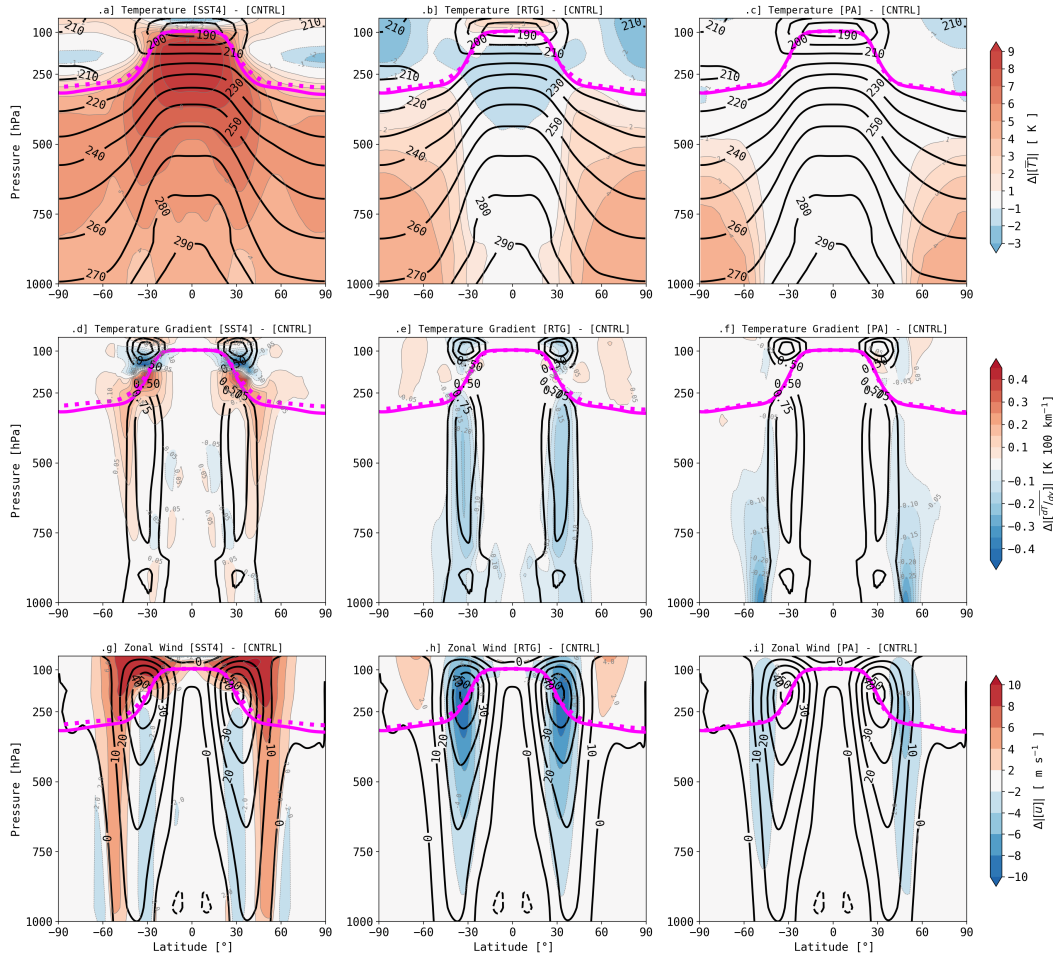


**Figure 2.** Atmospheric zonal mean climatologies of the ten year simulations. Shading shows the atmospheric responses ( $|\overline{[\text{EXPERIMENT}]}| - |\overline{[\text{CNTRL}]}|$ ) in temperature  $[\overline{T}]$  [K] (a, b, c), meridional temperature gradient  $[\overline{\frac{dT}{dy}}]$  [K 100 km<sup>-1</sup>] (d, e, f) and zonal wind  $[\overline{u}]$  [m s<sup>-1</sup>] (g, h, i) for the [SST4] simulation (column 1), [RTG] simulation (column 2) and [PA] simulation (column 3). Black contour lines represent the [CNTRL] simulation climatologies (labels indicate their values) and magenta contour lines the dynamical tropopause at the 2PVU surface — dashed magenta lines the equivalent in the experiment.

215 the polar edge of the baroclinic zone poleward as visible in the band of increased tem-  
 216 perature gradients and zonal winds in the mid-latitudes (Figures 2d and 2g).

### 217 **3.2 [RTG] simulation**

218 The [RTG] simulation warms in the lower to mid-troposphere at high latitudes, with  
 219 a maximum warming of approximately 4.5 K that extended into the mid-latitudes, from  
 220 where the warming gradually reduces to values of 1 K in the subtropics (Figure 2b). In  
 221 contrast to the upper tropical warming in the [SST4] simulation, the [RTG] simulation  
 222 shows cooling in this region. The cooling can be attributed to decreased latent heat re-  
 223 lease in the rising branch of the Hadley cells (not shown). The tropospheric warming in  
 224 the [RTG] simulation also results in a deeper troposphere, as indicated by the increased  
 225 height of the dynamic tropopause poleward of 30° latitude (Figure 2, column 2).

226 Overall, the effect of lower tropospheric polar warming and upper tropospheric trop-  
 227 ical cooling causes a substantial reduction in the tropospheric meridional temperature  
 228 gradient (Figure 2e). The strongest decrease up to 0.2 K 100 km<sup>-1</sup> occurs in the mid-  
 229 latitudes between 25° latitude and 50° latitude in the middle troposphere (Figure 2e).  
 230 In turn, the reduced meridional temperature gradient impacts the zonal circulation. Zonal  
 231 winds in the [RTG] simulation decrease substantially throughout the whole troposphere  
 232 (Figure 2h). Most prominently, the core of the jet stream weakens by approximately 15%  
 233 to 45.4 m s<sup>-1</sup>.

### 234 **3.3 [PA] simulation**

235 Compared to the [RTG] simulation, the warming of the lower to mid-troposphere  
 236 in the [PA] simulation is more confined to higher latitudes (Figure 2c). The maximum  
 237 warming of 4 K occurs poleward of 60° latitude in the lower troposphere, while equator-  
 238 ward of 45° latitude, the temperature response was neutral, ranging from -1 K to 1 K.

239 The most prominent effect of the low-level polar warming is the decrease in the merid-  
 240 ional temperature gradient on the poleward edge of the baroclinic zone in the mid-latitudes  
 241 up to 0.3 K 100 km<sup>-1</sup> near the surface (Figure 2f). This is the strongest tropospheric  
 242 meridional temperature-gradient reduction of all experiments and is expected from the  
 243 prescribed [PA] SST-profile (Figure 1a). The reduced temperature-gradient causes a de-  
 244 crease in zonal wind aloft, poleward of the jet stream core (Figure 2i). Apart from slightly  
 245 enhanced jet core strength from 1.1 m s<sup>-1</sup> to 54.4 m s<sup>-1</sup>, no notable wind speed changes  
 246 occur in the subtropics of the [PA] simulation.

## 247 **4 Jet Stream Waviness Response**

248 Next, we study the impact of the altered mean atmospheric state on wave ampli-  
 249 tudes, waviness of the jet stream, cut-off segment lengths and the variability within the  
 250 distributions of these diagnostics (Figure 3).

251 Our focus is on the extreme tails of the meridional extent and *SI* distributions, as-  
 252 sessed through changes in their respective 98<sup>th</sup> percentiles compared to the [CNTRL]  
 253 simulation (Figure 3). They correspond to large wave amplitudes and high waviness events  
 254 that are associated with weather extremes (e.g., Francis & Vavrus, 2015; Cattiaux et al.,  
 255 2016; Röthlisberger, Pfahl, & Martius, 2016; Coumou et al., 2018), and therefore more  
 256 societally relevant than the mean. To test if the 98<sup>th</sup> percentiles differ statistically sig-  
 257 nificantly we use the nonparametric quantile test (Johnson et al., 1987). We use the al-  
 258 ternative hypothesis ‘less’ which tests if the probability of the 98<sup>th</sup> percentile of the ex-  
 259 periment simulation has higher values than the [CNTRL] simulation. We also tested the  
 260 90<sup>th</sup> and 95<sup>th</sup> extreme percentiles (not shown) which gave qualitatively the same results  
 261 (except for the waviness and cut-off segments diagnostics in the [SST4] simulation). For

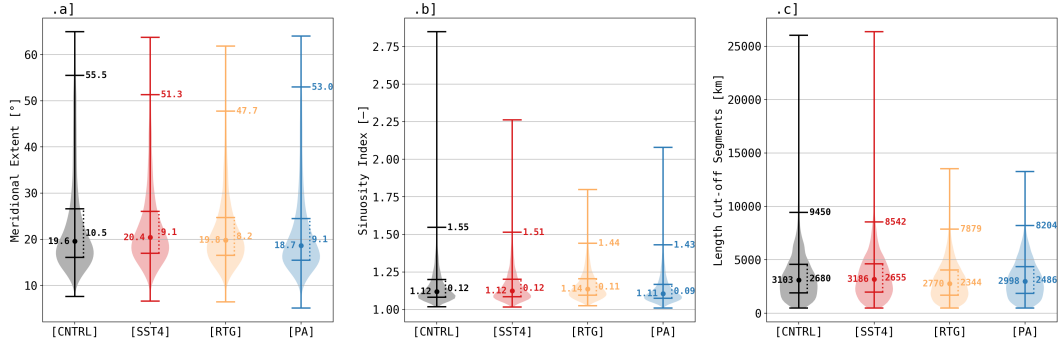


**Figure 3.** Violin plots for the 6-hourly distributions of (a) the meridional extent [°] of the average  $Z500$  in the latitudinal range of the selected  $Z500$  isohypses, (b) Sinuosity Index [-] and (c) the length of the cut-off segments of the selected  $Z500$  isohypses [km]. Labeled horizontal bars indicate the 98<sup>th</sup>, 75<sup>th</sup> and 25<sup>th</sup> percentile (from top to bottom), and the vertical dotted line represents the interquartile range.

262 completeness we also analyze the median (50<sup>th</sup> percentiles) of each diagnostic differs from  
 263 [CNTRL] using the Brown-Mood test.

264 Lastly, the variability in the distributions is studied by the interquartile ranges be-  
 265 cause the distributions are not normally distributed. To evaluate the statistical differ-  
 266 ences among these interquartile ranges, we employ bootstrapping. Comparisons among  
 267 the resulting distributions of the computed interquartile ranges (Figure S2) are conducted  
 268 using a student’s t-test.

269 Now, we first briefly discuss the general changes of the diagnostics supported by  
 270 statistical tests before we specifically highlight the most substantial changes found in each  
 271 simulation.

272 **4.1 General changes of the diagnostics**

273 Across all model experiments, and for each diagnostic, the 98<sup>th</sup> percentile of each  
 274 distribution show the most prominent changes (Figure 3). We find that the 98<sup>th</sup> percentiles  
 275 for each diagnostic is statistically significantly lower in the experiments compared to [CN-  
 276 CTRL] as confirmed by the quantile test at the 99% confidence interval.

277 The shifts in the medians are moderate and vary in sign. Despite the small mag-  
 278 nitude of the changes, they are statistically significantly different on the Brown-Mood  
 279 test at the 99% confidence interval for all diagnostics and simulations except for cut-off  
 280 segments length in [SST4] and [PA] (Table S1). However, all median changes are rela-  
 281 tively minor deviations compared to the natural variability depicted by the interquar-  
 282 tile ranges (Figure 3).

283 Interestingly, the interquartile ranges for each diagnostic in every simulation de-  
 284 creases compared to [CNTRL]. We find that the interquartile ranges for each diagnos-  
 285 tic is statistically significantly lower in the experiments compared to [CNTRL] as con-  
 286 firmed by the student’s t-test at the 99% confidence interval (Table S1). Hence, this re-  
 287 sult indicates a consistent reduction in variability of the selected diagnostics across all  
 288 warming scenarios.

289

## 4.2 [SST4] simulation

290

291

292

293

294

Comparing the meridional extent distribution between [SST4] and the [CNTRL] (Figure 3a), the 98<sup>th</sup> percentile decreases from 55.5° to 51.3°. Despite this decrease, the median of the distribution increases slightly from 19.6° to 20.4°. Thus, with uniform warming resulting in upper tropical warming and a strengthened jet stream, there is a robust decrease in the largest wave amplitudes and a slight increase in the median amplitude.

295

296

297

298

Analyzing the *SI* distribution (Figure 3b), the 98<sup>th</sup> percentile decreases from 1.55 in [CNTRL] to 1.51 in [SST4], indicating a decrease in extreme waviness episodes. There are no further alterations in the *SI* distribution, suggesting only a reduction in high-waviness episodes within [SST4].

299

300

301

302

Examining the cut-off segments distribution (Figure 3c), the 98<sup>th</sup> percentile signals a distinct reduction in the length of the longest cut-off segments under uniform warming. Marginal differences are observed in the median, indicating minimal changes in the lengths of cut-off segments of the [SST4] simulation.

303

## 4.3 [RTG] simulation

304

305

306

307

308

The changes observed in the extreme tail of the meridional extent distribution (Figure 3a) within [RTG] are most pronounced among all experiment simulations. The 98<sup>th</sup> percentile decreases from 55.5° in [CNTRL] to 47.7° in [RTG]. There is a marginal shift in the median towards higher values. Overall, these changes in the meridional extent of [RTG] suggest that the largest wave amplitudes are smaller in weaker jet streams.

309

310

311

312

313

314

315

Within the *SI* distribution (Figure 3b) of [RTG], consistent trends emerge. A notable decrease from 1.55 to 1.44 in the 98<sup>th</sup> percentile signifies a decrease in extreme waviness episodes. However, a marginal increase in *SI* of 0.02 in the median is observed. Consequently, weakened jet streams within [RTG] exhibit a distinct decrease in extreme waviness episodes alongside a slight increase in median waviness. This finding suggest that reduced low-level temperature gradients accompanied with weakened jet streams do not promote extreme waviness episodes.

316

317

318

Moreover, prominent reductions observed in the distribution depicting the length of cut-off segments (Figure 3c) within [RTG] indicate a consistent reduction in the length of these segments.

319

## 4.4 [PA] simulation

320

321

322

323

324

Polar warming stands out as the sole simulation consistently manifesting reductions across all distribution characteristics for each diagnostic (Figure 3). Notably, the 98<sup>th</sup> percentile of the meridional extent (Figure 3a) decreases from 55.5° in [CNTRL] to 53.0° in [PA]. While the median undergoes a robust yet marginal decrease, collectively, these outcomes suggest a reduction in wave amplitudes under polar warming conditions.

325

326

327

328

329

330

Similar consistent reductions are evident in the *SI* distributions (Figure 3b). The 98<sup>th</sup> percentile notably decreases from 1.55 in [CNTRL] to 1.43 in [PA], signifying a substantial decrease in extreme waviness episodes. Additionally, we find a minimal reduction in the median *SI* of 0.01. These reductions across all distribution characteristics collectively reinforce the evidence supporting decreased jet stream waviness under polar warming conditions.

331

332

333

Once again, in the characteristics related to the length of the cut-off segments (Figure 3c), analogous trends are observed. The 98<sup>th</sup> percentile and median display reductions in the length of the cut-off segments under polar warming conditions.

## 334 5 Discussion and Concluding Remarks

335 We perform four idealized aquaplanet simulations to study the causality between  
 336 large-scale spatial warming and jet stream extreme waviness. The results of the exper-  
 337 iments contribute to the open question whether the future jet stream is influenced by  
 338 large-scale spatial warming (e.g., Barnes & Screen, 2015; Shaw et al., 2016; Stendel et  
 339 al., 2021) and how jet stream waviness would alter (e.g., Vavrus, 2018; Coumou et al.,  
 340 2018; Cohen et al., 2020). To quantify jet stream waviness on an aquaplanet, we adjust  
 341 the latitudinal range and the normalization latitude in the computation of the Sinuos-  
 342 ity Index by Cattiaux et al. (2016). Using this waviness metric we are able to analyze  
 343 the length of cut-off segments, which are related to blocking highs and cut-off lows that  
 344 are associated with mid-latitude weather extremes (Cattiaux et al., 2016).

345 The idealized aquaplanet simulations generate robust responses in the mean zonal  
 346 climates of temperature, temperature gradients and zonal wind. Most notably, we find  
 347 substantial decreases in (large) wave amplitudes, (extreme) jet stream waviness and cut-  
 348 off segments for almost all simulations in each diagnostic. We enumerate the most promi-  
 349 nent results and highlight differences between the simulations:

- 350 1. In the [SST4] simulation, uniform warming of 4 K leads to upper tropospheric trop-  
 351 ical warming, enhanced meridional temperature gradients, and strengthened jet  
 352 streams. All three of the circulation diagnostics we consider show a significant de-  
 353 crease in their 98<sup>th</sup> percentiles and interquartile ranges, thus indicating the ex-  
 354 treme waviness events become less wavy and less variable with uniform warming.  
 355 The median of wave amplitudes, however, show a robust, but marginal increase.
- 356 2. Gradual warming from the equator to 5 K at the poles in the [RTG] simulation  
 357 substantially reduces meridional temperature gradients and weakens jet streams,  
 358 especially in the subtropical jet core region. All three of the circulation diagnos-  
 359 tics we consider depict even more significant decrease in their 98<sup>th</sup> percentiles in  
 360 [RTG]. This implies extreme waviness episodes become even less wavy and less  
 361 variable with meridional temperature gradient reductions. Also in [RTG] the me-  
 362 dian of wave amplitudes show a marginal increase.
- 363 3. Polar warming at high latitudes in the [PA] simulation reduces meridional tem-  
 364 perature gradients, primarily in the mid-latitudes and the lower troposphere, that  
 365 weakens jet streams aloft. The [PA] simulation consistently manifest reduction in  
 366 the 98<sup>th</sup> percentiles, medians and interquartile ranges across all three diagnostics.  
 367 This leads to robust reduced wave amplitudes, decreased waviness episodes and  
 368 reduced length of cut-off segments in conjunction with decreased variability.

369 Compared to [CNTRL], the reduced wave amplitudes observed in the [RTG] and  
 370 [PA] simulations align with findings from Hassanzadeh et al. (2014), who report a de-  
 371 crease in wave amplitude with reduced meridional temperature gradients in dry model  
 372 simulations. Furthermore, Hassanzadeh et al. (2014) find reduced areas affected by at-  
 373 mospheric blocking in simulations with reduced temperature gradients. While we did not  
 374 specifically detect blocking, our results indicate consistent findings with shortened cut-  
 375 off lengths in the reduced temperature gradient simulations [PA] and [RTG]. The only  
 376 highly idealized study that focuses on jet stream waviness specifically is Schemm and  
 377 Röthlisberger (2024). They find decreased waviness in 4 K uniform warmed aquaplanet  
 378 simulations with SSTs representing a summer and winter hemisphere. This is consistent  
 379 with what we find in [SST4].

380 The magnitude of all (statistically significant) responses in the median of [SST4],  
 381 [RTG] and [PA] is small compared to the natural variability of the [CNTRL] simulation.  
 382 This has previously been noted for reanalysis data (e.g., Barnes, 2013; Screen & Sim-  
 383 monds, 2013; Screen, 2014), comprehensive climate models (e.g., Cattiaux et al., 2016),

384 models with induced sea-ice loss alone (e.g., Blackport & Screen, 2020; Smith et al., 2022)  
385 and highly idealized simulations (Hassanzadeh et al., 2014; Schneider et al., 2015).

386 Additionally, the natural variability reduces as evidenced by the robust decrease  
387 in the interquartile range of the distributions of wave amplitude, jet stream waviness and  
388 cut-off segments. This suggests that large-scale spatial warming makes the atmospheric  
389 circulation less variable. The reduced variability in the experiment simulations is poten-  
390 tially caused by weakened baroclinicity and, hence, the jet stream is less affected by syn-  
391 optoc waves. Schemm and Röthlisberger (2024) find a reduction of synoptic wave am-  
392 plitude with uniform warming and state that these waves play a more substantial role  
393 in shaping the geometric waviness of the jet stream. Indeed, Sinclair and Catto (2023),  
394 with identical [SST4] and [PA] simulations, find for uniform warming weakened Eady  
395 growth rates and for polar amplification weakened growth rates in the low-to-middle tro-  
396 posphere on the poleward side of the jet, but slight increases in the mid-to-upper tro-  
397 posphere at high latitudes. For our [RTG] simulation we expect even larger reductions  
398 in baroclinicity because the natural variability is the lowest in all simulations.

399 Our results contradict the mechanism proposed by Francis and Vavrus (2012, 2015),  
400 that a reduced temperature gradient, consequently, a weaker zonal flow, would lead to  
401 amplified and more wavy jet streams, resulting in increased weather extremes. Their hy-  
402 pothesis, however, leans on the linearity assumption of barotropic Rossby wave theory,  
403 which may not fully encompass the highly nonlinear behavior observed in the real at-  
404 mosphere and the aquaplanet’s atmosphere. This might be because barotropic Rossby  
405 wave theory does not describe nonlinear baroclinic growth of synoptic waves.

406 Another possible explanation for these results contradicting the mechanism pro-  
407 posed by Francis and Vavrus (2012, 2015), is the use of an aquaplanet where the absence  
408 of zonal asymmetries, like orography and land-sea contrasts, eliminates many Rossby wave  
409 sources. Moon et al. (2022), have identified thermal forcing, arising from land-sea con-  
410 trasts, in conjunction with weakened flow, as pivotal factors for generating wavier jet streams.  
411 Thus, future idealized experiments could introduce extra complexity by introducing SST  
412 perturbations (Brayshaw et al., 2008; Schemm et al., 2022), simple continents (Brayshaw  
413 et al., 2009), orography or all these aspects (Brayshaw et al., 2011) in combination with  
414 temperature gradient reductions. This approach could provide a more comprehensive un-  
415 derstanding of the impact of temperature gradient modifications on jet stream circula-  
416 tion changes and increased weather extremes.

417 In summary, results from our study demonstrates that large-scale spatial warm-  
418 ing on an aquaplanet affects meridional temperature gradients and jet streams. Both strength-  
419 ened and weakened jet streams show robust decreases in the magnitudes of large wave  
420 amplitudes and extreme episodes of jet stream waviness. We suggest that these results  
421 are related to reduced baroclinicity in all simulations. Ultimately, we conclude that weaker  
422 jet streams do not necessarily become wavier.

## 423 6 Open Research

424 Data archiving is underway. We plan to archive at Zenodo.

## 425 Acknowledgments

426 The authors want to thank ECMWF for making OpenIFS available to the University  
427 of Helsinki and Wageningen University. The simulations were carried out on the Dutch  
428 national supercomputer Snellius with the support of SURF ([www.surf.nl](http://www.surf.nl), project num-  
429 ber NWO-2023.003). VAS was supported by the Research Council of Finland (grant no  
430 338615).

431 **References**

- 432 Barnes, E. A. (2013). Revisiting the evidence linking arctic amplification to extreme  
433 weather in midlatitudes. *Geophysical research letters*, *40*(17), 4734–4739.
- 434 Barnes, E. A., & Polvani, L. M. (2015). CMIP5 Projections of Arctic Amplification,  
435 of the North American/North Atlantic Circulation, and of Their Relationship.  
436 *Journal of Climate*, *28*(13), 5254–5271. (Publisher: American Meteorological  
437 Society Section: Journal of Climate) doi: 10.1175/JCLI-D-14-00589.1
- 438 Barnes, E. A., & Screen, J. A. (2015). The impact of Arctic warming on the midlat-  
439 itude jet-stream: Can it? Has it? Will it? *WIREs Climate Change*, *6*(3), 277–  
440 286. doi: 10.1002/wcc.337
- 441 Blackport, R., & Screen, J. A. (2020). Insignificant effect of arctic amplification  
442 on the amplitude of midlatitude atmospheric waves. *Science advances*, *6*(8),  
443 eaay2880.
- 444 Brayshaw, D. J., Hoskins, B., & Blackburn, M. (2008). The storm-track response to  
445 idealized sst perturbations in an aquaplanet gcm. *Journal of the Atmospheric  
446 Sciences*, *65*(9), 2842–2860.
- 447 Brayshaw, D. J., Hoskins, B., & Blackburn, M. (2009). The basic ingredients of the  
448 north atlantic storm track. part i: Land–sea contrast and orography. *Journal  
449 of the Atmospheric Sciences*, *66*(9), 2539–2558.
- 450 Brayshaw, D. J., Hoskins, B., & Blackburn, M. (2011). The basic ingredients of the  
451 north atlantic storm track. part ii: Sea surface temperatures. *Journal of the  
452 Atmospheric Sciences*, *68*(8), 1784–1805.
- 453 Butler, A. H., Thompson, D. W. J., & Heikes, R. (2010). The Steady-State Atmo-  
454 spheric Circulation Response to Climate Change–like Thermal Forcings in a  
455 Simple General Circulation Model. *Journal of Climate*, *23*(13), 3474–3496.  
456 doi: 10.1175/2010JCLI3228.1
- 457 Cattiaux, J., Peings, Y., Saint-Martin, D., Trou-Kechout, N., & Vavrus, S. J. (2016).  
458 Sinuosity of midlatitude atmospheric flow in a warming world. *Geophysical Re-  
459 search Letters*, *43*(15), 8259–8268.
- 460 Chen, G., Lu, J., Burrows, D. A., & Leung, L. R. (2015). Local finite-amplitude  
461 wave activity as an objective diagnostic of midlatitude extreme weather. *Geo-  
462 physical Research Letters*, *42*(24), 10–952.
- 463 Cohen, J., Zhang, X., Francis, J., Jung, T., Kwok, R., Overland, J., . . . others  
464 (2020). Divergent consensus on arctic amplification influence on midlatitude  
465 severe winter weather. *Nature Climate Change*, *10*(1), 20–29.
- 466 Coumou, D., Di Capua, G., Vavrus, S., Wang, L., & Wang, S. (2018). The influence  
467 of arctic amplification on mid-latitude summer circulation. *Nature Communi-  
468 cations*, *9*(1), 2959.
- 469 Di Capua, G., & Coumou, D. (2016). Changes in meandering of the northern hemi-  
470 sphere circulation. *Environmental Research Letters*, *11*(9), 094028.
- 471 Doblas-Reyes, F., Sörensson, A., Almazroui, M., Dosio, A., Gutowski, W., Haarsma,  
472 R., . . . Zuo, Z. (2021). Linking global to regional climate change [Book  
473 Section]. In V. Masson-Delmotte et al. (Eds.), *Climate change 2021: The  
474 physical science basis. contribution of working group i to the sixth assessment  
475 report of the intergovernmental panel on climate change* (p. 1363–1512). doi:  
476 10.1017/9781009157896.012
- 477 Francis, J. A., & Vavrus, S. J. (2012). Evidence linking arctic amplification to ex-  
478 treme weather in mid-latitudes. *Geophysical research letters*, *39*(6).
- 479 Francis, J. A., & Vavrus, S. J. (2015). Evidence for a wavier jet stream in response  
480 to rapid Arctic warming. *Environmental Research Letters*, *10*(1), 014005. doi:  
481 10.1088/1748-9326/10/1/014005
- 482 Gulev, S., Thorne, P., Ahn, J., Dentener, F., Domingues, C., Gerland, S., . . .  
483 Vose, R. (2021). Changing state of the climate system [Book Section].  
484 In V. Masson-Delmotte et al. (Eds.), *Climate change 2021: The physical  
485 science basis. contribution of working group i to the sixth assessment re-*

- 486 port of the intergovernmental panel on climate change (p. 287–422). doi:  
487 10.1017/9781009157896.004
- 488 Hassanzadeh, P., Kuang, Z., & Farrell, B. F. (2014). Responses of midlatitude  
489 blocks and wave amplitude to changes in the meridional temperature gradient  
490 in an idealized dry gcm. *Geophysical Research Letters*, *41*(14), 5223–5232.
- 491 Hersbach, H., Bell, B., Berrisford, P., Hirahara, S., Horányi, A., Muñoz-Sabater, J.,  
492 ... others (2020). The era5 global reanalysis. *Quarterly Journal of the Royal  
493 Meteorological Society*, *146*(730), 1999–2049.
- 494 IPCC. (2021). *Climate change 2021: The physical science basis. contribution of  
495 working group i to the sixth assessment report of the intergovernmental panel  
496 on climate change* [Book]. doi: 10.1017/9781009157896
- 497 Johnson, R. A., Verrill, S., & Moore, D. H. (1987). Two-sample rank tests for de-  
498 tecting changes that occur in a small proportion of the treated population.  
499 *Biometrics*, 641–655.
- 500 Lee, J.-Y., Marotzke, J., Bala, G., Cao, L., Corti, S., Dunne, J., ... Zhou, T. (2021).  
501 Future global climate: Scenario-based projections and near-term information  
502 [Book Section]. In V. Masson-Delmotte et al. (Eds.), *Climate change 2021:  
503 The physical science basis. contribution of working group i to the sixth assess-  
504 ment report of the intergovernmental panel on climate change* (p. 553–672).  
505 doi: 10.1017/9781009157896.006
- 506 Martin, J. E. (2021). Recent Trends in the Waviness of the Northern Hemisphere  
507 Wintertime Polar and Subtropical Jets. *Journal of Geophysical Research: At-  
508 mospheres*, *126*(9), e2020JD033668. doi: 10.1029/2020JD033668
- 509 Moon, W., Kim, B.-M., Yang, G.-H., & Wettlaufer, J. S. (2022). Wavier jet streams  
510 driven by zonally asymmetric surface thermal forcing. *Proceedings of the Na-  
511 tional Academy of Sciences*, *119*(38), e2200890119.
- 512 Mori, M., Kosaka, Y., Watanabe, M., Nakamura, H., & Kimoto, M. (2019). A recon-  
513 ciled estimate of the influence of Arctic sea-ice loss on recent Eurasian cooling.  
514 *Nature Climate Change*, *9*(2), 123–129. doi: 10.1038/s41558-018-0379-3
- 515 Neale, R. B., & Hoskins, B. J. (2000). A standard test for agcms including their  
516 physical parametrizations: I: The proposal. *Atmospheric Science Letters*, *1*(2),  
517 101–107.
- 518 Ogawa, F., Keenlyside, N., Gao, Y., Koenigk, T., Yang, S., Suo, L., ... Semenov,  
519 V. (2018). Evaluating Impacts of Recent Arctic Sea Ice Loss on the Northern  
520 Hemisphere Winter Climate Change. *Geophysical Research Letters*, *45*(7),  
521 3255–3263. doi: 10.1002/2017GL076502
- 522 Peings, Y., Cattiaux, J., Vavrus, S., & Magnusdottir, G. (2017). Late Twenty-  
523 First-Century Changes in the Midlatitude Atmospheric Circulation in the  
524 CESM Large Ensemble. *Journal of Climate*, *30*(15), 5943–5960. doi:  
525 10.1175/JCLI-D-16-0340.1
- 526 Röthlisberger, M., Martius, O., & Wernli, H. (2016). An algorithm for identifying  
527 the initiation of synoptic-scale Rossby waves on potential vorticity waveguides.  
528 *Quarterly Journal of the Royal Meteorological Society*, *142*(695), 889–900. doi:  
529 10.1002/qj.2690
- 530 Röthlisberger, M., Pfahl, S., & Martius, O. (2016). Regional-scale jet waviness mod-  
531 ulates the occurrence of midlatitude weather extremes. *Geophysical Research  
532 Letters*, *43*(20), 10,989–10,997. doi: 10.1002/2016GL070944
- 533 Schemm, S., Papritz, L., & Rivière, G. (2022). Storm track response to uniform  
534 global warming downstream of an idealized sea surface temperature front.  
535 *Weather and Climate Dynamics*, *3*(2), 601–623.
- 536 Schemm, S., & Röthlisberger, M. (2024). Aquaplanet simulations with winter  
537 and summer hemispheres: model setup and circulation response to warming.  
538 *Weather and Climate Dynamics*, *5*(1), 43–63. doi: 10.5194/wcd-5-43-2024
- 539 Schneider, T., Bischoff, T., & Plotka, H. (2015). Physics of changes in synoptic mid-  
540 latitude temperature variability. *Journal of Climate*, *28*(6), 2312–2331.

- 541 Screen, J. A. (2014). Arctic amplification decreases temperature variance in north-  
542 ern mid-to high-latitudes. *Nature Climate Change*, *4*(7), 577–582.
- 543 Screen, J. A., Deser, C., Smith, D. M., Zhang, X., Blackport, R., Kushner, P. J., ...  
544 Sun, L. (2018). Consistency and discrepancy in the atmospheric response to  
545 arctic sea-ice loss across climate models. *Nature Geoscience*, *11*(3), 155–163.
- 546 Screen, J. A., & Simmonds, I. (2013). Exploring links between Arctic amplification  
547 and mid-latitude weather. *Geophysical Research Letters*, *40*(5), 959–964. doi:  
548 10.1002/grl.50174
- 549 Shaw, T. A., Baldwin, M., Barnes, E. A., Caballero, R., Garfinkel, C. I., Hwang,  
550 Y.-T., ... Voigt, A. (2016). Storm track processes and the opposing influences  
551 of climate change. *Nature Geoscience*, *9*(9), 656–664. doi: 10.1038/ngeo2783
- 552 Sinclair, V. A., & Catto, J. L. (2023). The relationship between extra-tropical  
553 cyclone intensity and precipitation in idealised current and future climates.  
554 *Weather and Climate Dynamics*, *4*(3), 567–589. doi: 10.5194/wcd-4-567-2023
- 555 Sinclair, V. A., Rantanen, M., Haapanala, P., Räisänen, J., & Järvinen, H.  
556 (2020). The characteristics and structure of extra-tropical cyclones in  
557 a warmer climate. *Weather and Climate Dynamics*, *1*(1), 1–25. doi:  
558 10.5194/wcd-1-1-2020
- 559 Smith, D. M., Eade, R., Andrews, M., Ayres, H., Clark, A., Chripko, S., ... others  
560 (2022). Robust but weak winter atmospheric circulation response to future  
561 arctic sea ice loss. *Nature communications*, *13*(1), 727.
- 562 Smith, D. M., Screen, J. A., Deser, C., Cohen, J., Fyfe, J. C., García-Serrano, J.,  
563 ... others (2019). The polar amplification model intercomparison project  
564 (pamip) contribution to cmip6: investigating the causes and consequences of  
565 polar amplification. *Geoscientific Model Development*, *12*(3), 1139–1164.
- 566 Stendel, M., Francis, J., White, R., Williams, P. D., & Woollings, T. (2021). Chap-  
567 ter 15 - The jet stream and climate change. In T. M. Letcher (Ed.), *Climate*  
568 *Change (Third Edition)* (pp. 327–357). doi: 10.1016/B978-0-12-821575-3.00015  
569 -3
- 570 Vallis, G. K. (2020). The Trouble with Water: Condensation, Circulation and Cli-  
571 mate. *The European Physical Journal Plus*, *135*(6), 478. doi: 10.1140/epjp/  
572 s13360-020-00493-7
- 573 Vavrus, S. J. (2018). The influence of arctic amplification on mid-latitude weather  
574 and climate. *Current Climate Change Reports*, *4*, 238–249.
- 575 Woollings, T., Barriopedro, D., Methven, J., Son, S.-W., Martius, O., Harvey, B., ...  
576 Seneviratne, S. (2018). Blocking and its response to climate change. *Current*  
577 *climate change reports*, *4*, 287–300.
- 578 Woollings, T., Drouard, M., O'Reilly, C. H., Sexton, D. M., & McSweeney, C.  
579 (2023). Trends in the atmospheric jet streams are emerging in observations  
580 and could be linked to tropical warming. *Communications Earth & Environ-*  
581 *ment*, *4*(1), 125.